Metastability in Schloegl's second model for autocatalysis: Lattice-gas realization with particle diffusion

Xiaofang Guo,[1] Y. De Decker,[2] and J. W. Evans[1]

[1]*Ames Laboratory–US DOE, and Department of Physics & Astronomy and Department of Mathematics, Iowa State University, Ames, Iowa 50011, USA*

[2]*Interdisciplinary Center for Nonlinear Phenomena and Complex Systems, Université Libre de Bruxelles, Campus Plaine, Code Postal 231, B-1050 Brussels, Belgium*

We analyze metastability associated with a discontinuous nonequilibrium phase transition in a stochastic lattice-gas realization of Schloegl's second model for autocatalysis. This model realization involves spontaneous annihilation, autocatalytic creation, and diffusion of particles on a square lattice, where creation at empty sites requires an adjacent diagonal pair of particles. This model, also known as the quadratic contact process, exhibits discontinuous transition between a populated active state and a particle-free vacuum or "poisoned" state, as well as generic two-phase coexistence. The poisoned state exists for all particle annihilation rates $p > 0$ and hop rates $h \geq 0$ and is an absorbing state in the sense of Markovian processes. The active or reactive steady state exists only for p below a critical value, $p_e = p_e(h)$, but a metastable extension appears for a range of higher p up to an effective upper spinodal point, $p_{s+} = p_{s+}(h)$ (i.e., $p_{s+} > p_e$). For selected h, we assess the location of $p_{s+}(h)$ by characterizing both the poisoning kinetics and the propagation of interfaces separating vacuum and active states as a function of p.

PACS number(s): 05.70.Fh, 82.40.Bj, 05.50.+q, 05.70.Ln

I. INTRODUCTION

There has been long-standing interest in discontinuous phase transitions for systems in thermodynamic equilibrium, and particularly in associated metastability and nucleation phenomena [1,2]. For example, in the mean-field van der Waals description of a fluid below a critical temperature, one finds van der Waals loops. These loops reflect phase separation where a stable high-density liquid state exists for pressures above an equistability pressure for coexistence with a dilute gas state. This stable liquid state extends to a metastable liquid state for a range of lower pressures down to a well-defined spinodal point [3]. The equistability pressure is determined by a Maxwell construction. In statistical-mechanical analyses of fluid systems, the equistability pressure corresponds to the location of a discontinuous transition. Furthermore, these analyses indicate a dependence of spinodal behavior on system size [1,2]. In fact, for the equilibrium Ising model for an infinite system [4–6], it has been shown that there does not exist a unique analytical extension of the stable steady state to a metastable state. It is possible to generate a family of C^∞ metastable extensions by running an appropriate choice of model dynamics from a suitable initial state for a period of time increasing exponentially with the inverse distance from the equistability point [4–6]. However, this family of extensions does not provide much insight into the location of any effective spinodal point for an infinite system. Indeed, there is no natural unique definition of such a spinodal point for these equilibrium thermodynamic systems.

Nonequilibrium systems provide an even richer variety of phase transition or bifurcation behavior [7,8] than equilibrium systems, although there are also strong analogies. Mean-field analysis often reveals bistability of nonequilibrium steady states providing the analog of van der Waals loops. The boundary of the nonequilibrium bistable regime at a saddle-node bifurcation corresponds to an equilibrium spinodal point. The complete disappearance of nonequilibrium bistability at a cusp bifurcation is the analog of an equilibrium critical point [8,9].

A natural goal for such nonequilibrium systems is to advance beyond the mean-field level to statistical-mechanical analyses. Along these lines, there are a large number of studies of nonequilibrium continuous phase transitions in lattice-gas models which have focused on universality [10–12]. However, increasing attention is being paid to analysis of various phenomena in reaction–diffusion-type models exhibiting discontinuous transitions: propagation and fluctuation behavior of interfaces between active and poisoned states [13–18], epidemic properties of an active droplet embedded in an absorbing or poisoned state [19,20], and nucleation of droplets within a metastable active state [14,18,21].

It is well recognized that lattice-gas reaction-diffusion models with discontinuous transitions exhibit metastability [9]. However, just as for equilibrium systems, one does not expect the existence of a unique analytical extension of stable states to metastable states beyond transition points, and thus one does not expect spinodal points to be uniquely or well defined for infinite systems [24,25]. Nonetheless, the concept of a spinodal provides a valuable tool for interpretation of model dynamics, so further analysis is appropriate. Interestingly, for nonequilibrium systems, there exist both additional challenges and advantages relative to equilibrium systems. The challenges derive from the feature that there does not exist a thermodynamic framework for analysis of these systems, so, e.g., critical droplets within the metastable state cannot be described in terms of a free-energy functional [1]. On the other hand, for models exhibiting mean-field bistability, one can recover true bistability in the statistical-mechanical model in the regime of rapid hopping of at least

one type of reactant particle. In this regime of "efficient stirring," spinodal points can become perfectly well defined just as in a mean-field theory (even if spatial correlations persist in the model) [9,22].

In this study, we consider Schloegl's second model for autocatalysis in a reactive system of particles, X. This model traditionally includes the following mechanistic steps [8,16–18,23–27]:

$$X \rightarrow \varnothing \text{ (spontaneous annihilation),}$$

$$2X \rightarrow 3X \text{(autocatalytic creation).} \quad (1)$$
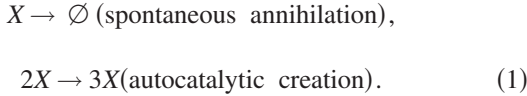
Spontaneous annihilation occurs at rate p, and autocatalytic creation requires existing nearby pairs of particles (and occurs at suitably prescribed rates, as discussed below). The most general formulation of the model also includes spontaneous creation $\varnothing \rightarrow X$, but this process is excluded in our study. Traditional off-lattice formulations also include the autocatalytic annihilation process $3X \rightarrow 2X$ in order to avoid population explosion [8,23]. However, in lattice formulations, autocatalytic particle creation requires an empty site $\varnothing$, which automatically limits population growth. Thus, particle creation in the lattice model is more accurately represented as $2X + \varnothing \rightarrow 3X$ [16–18,26,27]. Particle diffusion is typically operative.

Both off-lattice and lattice formulations display cubic mean-field kinetics, i.e., the rate of change of particle concentration C is a cubic function of C [8,18,23,27]. Upon increasing the annihilation rate p, there is a bifurcation in the steady states from mean-field bistability (where a stable active steady state with finite population $C>0$ coexists with the stable $C=0$ vacuum state) to monostability (where the vacuum state is the unique stable steady state) [18].

In this contribution, we will restrict our attention to a statistical-mechanical analysis of a specific realization of Schloegl's second model on a square lattice with particle hopping at rate $h \geq 0$, which is also known as the quadratic contact process (QCP) [16–18,27]. This realization displays a discontinuous transition from an active state to the vacuum state when p exceeds $p_e(h)$. One also finds evidence for a metastable extension of the active steady state into a regime $p_e(h) \leq p \leq p_{s+}(h)$, where $p_{s+}(h)$ denotes an effective upper spinodal point. This spinodal point is of particular interest in our study. We extend previous investigations [18] by providing other more reliable simulation strategies to estimate $p_{s+}(h)$, a comprehensive analytical investigation of the lattice model at the level of the pair approximation, and suggest a coarse-grained modeling strategy to describe non-mean-field model behavior. Our focus here is exclusively on behavior in the limit of infinite system size, rather than considering finite systems where a variety of approaches to defining spinodals have been considered [1,28]. For completeness, we note that this model also displays "generic two-phase coexistence" of stable active and vacuum states for a finite range $p_f(h) \leq p \leq p_e(h)$, where $p_e(h) - p_f(h) \rightarrow 0$ "quickly," as h increases above zero [18].

In Sec. II, we describe in detail the realization of the QCP analyzed in this paper, and also present the hierarchical form of the exact master equation for this model. In Sec. III, we
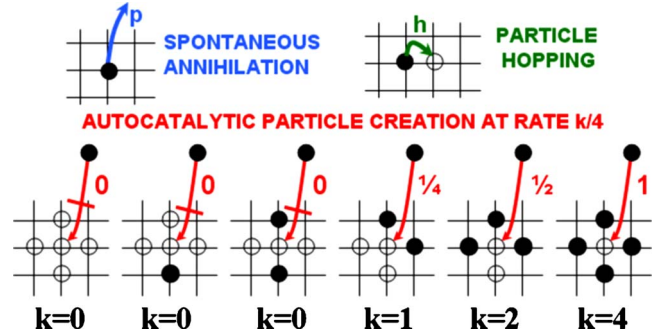

FIG. 1. (Color online) Schematic of particle annihilation, autocatalytic creation, and hopping processes in Schloegl's second model or the QCP on a square lattice. Particles are denoted by filled circles (●) and empty sites are denoted by open circles (○). Rates for the various processes are also indicated, and the bar through the arrow indicates that the process is inactive.

present simulation results for "moderate" hop rate. We analyze both the poisoning kinetics in the vicinity of the effective spinodal point and the propagation of interfaces separating active and vacuum states. Next, in Sec. IV, we present an analysis of the above two features of model behavior within the pair approximation to the exact master equations. This facilitates the interpretation of the simulation results. Finally, in Sec. V, we discuss the development of coarse-grained continuum Langevin reaction-diffusion equations (RDEs) describing the model at a level beyond the traditional mean-field site approximation. Specifically, these RDEs are based on the pair approximation and can thus more accurately describe reaction kinetics for moderate h. Finally, conclusions are provided in Sec. VI.

II. MODEL SPECIFICATION AND HIERACHICAL MASTER EQUATIONS

Our realization of Schloegl's second model, or equivalently of the QCP, on a square lattice as a stochastic Markovian process involves the following components [18–27]: (i) particle annihilation occurring randomly at rate p; (ii) particle creation at empty sites requiring one or more diagonally adjacent pairs of occupied sites; specifically, the creation rate is given by $k/4$, where k is the number of adjacent diagonal occupied pairs and thus can take the value of $k=0$, 1, 2, or 4; and (iii) hopping of particles to any adjacent empty sites at rate h (per target site). Figure 1 provides a schematic of these processes. Again C denotes the particle concentration, i.e., the fraction of filled or occupied sites. For any $p>0$, the "vacuum state" with $C=0$ corresponds to an absorbing steady state from which the system cannot escape. However, there also exists an active or reactive steady state with $C=C_{eq}(p)>0$ for $0<p \leq p_e(h)$, and our focus in this work will be on the metastable state which "extends" this active state into the regime $p_e(h)<p<p_{s+}(h)$ for some ill-defined $p_{s+}(h)$ [see Fig. 2(a)].

Note that for $p \ll 1$, the lattice is almost completely populated in the active state. Thus, effectively particle creation occurs at empty sites with rate 1, and as a result one has
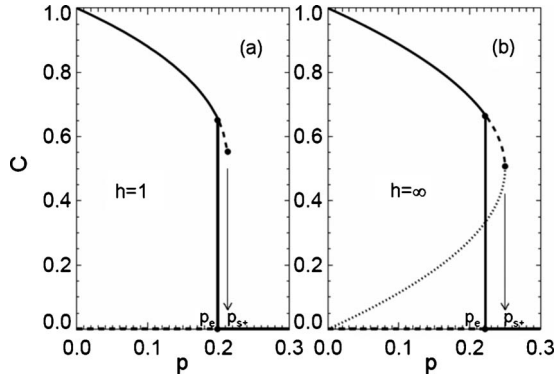
FIG. 2. Steady-state behavior for the particle concentration $C_{eq}(p)$ versus p in the QCP with particle hopping at rate h. Plots show stable steady states as solid lines, metastable steady states as dashed lines, and indicate the locations of p_e and p_{s+}: (a) $h=1$ (simulation results); (b) $h=\infty$ (exact mean-field behavior with an unstable steady state shown as a dotted line).

$C_{eq}(p)=1-p+O(p^2)$, independent of h. In the limit $h \to \infty$, "rapid stirring" will destroy all spatial correlations given the lack of interactions between particles in this model. Thus, traditional mean-field kinetics will apply where $C_{eq}(p)=\frac{1}{2}+\frac{1}{2}(1-4p)^{1/2}$ and $p_e(\infty)=2/9$ as explained in Sec. II C [18]. Also, as $h \to \infty$, the lifetime of the metastable state will diverge, so one recovers a regime of true bistability terminated by a well-defined upper spinodal, $p_{s+}(\infty)=1/4$ [9,18].

While kinetic Monte Carlo (KMC) simulation will be utilized below to provide precise results for the behavior of C for finite hop rate h, it is instructive to present the exact master equation for the QCP with $h \geq 0$ in the form of an infinite coupled hierarchy [29]. It will be useful to explore the predictions of truncation approximations to these equations. Here, we fully enumerate and simplify these equations for spatially homogeneous states, but just present the simplified version of the equations for the more general case of spatially inhomogeneous states.

A. Spatially homogeneous states

First, consider spatially homogeneous states of the QCP with $h \geq 0$ on an infinite square lattice. Here, "spatially homogenous" means in a statistical or ensemble averaged sense. Individual realizations of the process exhibit spatial correlations and fluctuations. We let "x" denote an occupied site and "o" denote an empty site. Then, $P[x]=C$ denotes the probability of an occupied site, $P[o]=1-C$ denotes the probability of an empty site, $P[x\ x]$ denotes the probability of an adjacent occupied pair, $P[o\ o]$ denotes the probability of an adjacent empty pair, $P[o-o]$ denotes the probability of an empty pair separated by a site of unspecified state, etc. Conservation of probability ensures that all configurational probabilities can be written as combinations of such probabilities for configurations with just empty sites, e.g., $P[x]=1-P[o]$, $P[x\ o]=P[o]-P[o\ o]$, $P[x\ x]=1-2P[o]+P[o\ o]$, etc. [30]. Alternatively, one could write all configurational probabilities in terms of those with just occupied-site configurations. For the QCP, we favor empty site configurations when

developing the master equations. This facilitates more substantial simplification of the form of the equations, as illustrated below. Empty site configurations were similarly favored in analysis of models which include just irreversible cooperative creation of particles (with no annihilation or hopping), usually referred to as "cooperative sequential adsorption" models [30]. The exact form of the first two such hierarchical master equations in an infinite coupled set becomes

$$
\begin{aligned}
d/dt\,P[o] &= p \times P[x] - \left(4 \times \frac{1}{4} \times P\!\left[\begin{smallmatrix} & x & \\ o & o & x \\ & o & \end{smallmatrix}\right] \right. \\
&\quad \left. + 4 \times \frac{1}{2} \times P\!\left[\begin{smallmatrix} & x & \\ o & o & x \\ & x & \end{smallmatrix}\right] + 1 \times 1 \times P\!\left[\begin{smallmatrix} & x & \\ x & o & x \\ & x & \end{smallmatrix}\right] \right) \\
&= p \times P[x] - P\!\left[\begin{smallmatrix} & x & \\ o & x & \end{smallmatrix}\right],
\end{aligned}
\tag{2a}
$$

$$
\begin{aligned}
d/dt\,P[o\ o] &= 2p \times P[o\ x] - 2 \times \left(2 \times \frac{1}{4} \times P\!\left[\begin{smallmatrix} & x & \\ o & o & x \\ & o & \end{smallmatrix}\right] \right. \\
&\quad \left. + 1 \times \frac{1}{2} \times P\!\left[\begin{smallmatrix} & x & \\ o & o & x \\ & x & \end{smallmatrix}\right] \right) \\
&\quad + 2h \times \left(P[o\ x\ o] \right. \\
&\quad + 2 \times P\!\left[\begin{smallmatrix} & o & \\ o & x & \end{smallmatrix}\right] - P[o\ o\ x] \\
&\quad \left. - 2 \times P\!\left[\begin{smallmatrix} & x & \\ o & o & \end{smallmatrix}\right] \right) \\
&= 2p \times P[o\ x] - P\!\left[\begin{smallmatrix} & x & \\ o & o & x \end{smallmatrix}\right] \\
&\quad + 2h \times \left(P[o\ -\ o] + 2 \times P\!\left[\begin{smallmatrix} & o & \\ o & - & \end{smallmatrix}\right] \right. \\
&\quad \left. - 3 \times P[o\ o] \right).
\end{aligned}
\tag{2b}
$$

The first gain terms in Eqs. (2a) and (2b) (proportional to p) correspond to particle annihilation. The second group of loss terms after the first equality corresponds to autocatalytic creation. The integer prefactor indicates the number of equivalent configurations (accounting for rotational symmetries), and the fractional prefactor indicates the associated creation rate.

An exact reduction of this group of contributions is possible due to the specific values selected for the creation rates [29] and is shown after the second equality. Particle hopping terms are absent in the $P[o]$ equation since hopping preserves particle number. However, such contributions do appear as the last group of terms (proportional to h) in the

$P[o\ o]$ equation (2b). The complete form of these terms, shown after the first equality, includes both gain terms due to a particle hopping out of one site of the pair of sites of interest to a neighboring empty site, thus creating an empty pair. There are also loss terms due to a particle hopping onto the empty pair of interest. An exact simplification is possible for these hopping terms exploiting conservation of probability [31], and this is shown after the second equality in Eq. (2b). Again the integer prefactor indicates the number of equivalent contributions.

It should be noted that these exact hierarchical equations consistently recover mean-field kinetics in the limit $h \to \infty$ where all multisite configurational probabilities factor as products of constituent single-site probabilities. This reduction is clearly realized and quantified at the level of higher-order truncation approximations to the hierarchical equations as described in Sec. IV.

B. Spatially inhomogeneous states

For a more complete analysis of model behavior, one can extend the above hierarchical master equations to consider spatially nonuniform or inhomogeneous states in an infinite system [29]. As above, this characterization refers to ensemble averaged states. In particular, one can use these generalized equations to analyze the propagation of planar interfaces separating vacuum and active states to determine annihilation rates $p = p_{eq}(h, S)$, corresponding to stationarity of these interfaces (which here depend on the slope or orientation S of the interface).

To this end, we introduce location-dependent probabilities for specific configurations of sites, e.g., $P[o_{i,j}]$ for the probability that site (i,j) is empty, $P[o_{i,j}\ o_{i+1,j}]$ for the probability that the adjacent pair of sites (i,j) and $(i+1,j)$ are both empty, an analogous quantity for the probability of a vertical pair of empty sites, etc. Then, after exact reduction or simplification of the type described above for uniform states, the first two equations in the exact set of hierarchical master equations describing the evolution of these quantities have the form

$$d/dt\,P[o_{i,j}] = pP[x_{i,j}] - \frac{1}{4}P\begin{bmatrix} & x_{i,j+1} & \\ o_{i,j} & & x_{i+1,j} \end{bmatrix}$$
$$- \frac{1}{4}P\begin{bmatrix} o_{i,j} & x_{i+1,j} \\ x_{i,j-1} & \end{bmatrix} - \frac{1}{4}P\begin{bmatrix} & x_{i,j+1} \\ x_{i-1,j} & o_{i,j} \end{bmatrix}$$
$$- \frac{1}{4}P\begin{bmatrix} x_{i-1,j} & o_{i,j} \\ & x_{i,j-1} \end{bmatrix} + h(P[o_{i+1,j}] + P[o_{i-1,j}]$$
$$+ P[o_{i,j+1}] + P[o_{i,j-1}] - 4P[o_{i,j}]), \tag{3a}$$

$$d/dt\,P[o_{i,j}\ o_{i+1,j}] = pP[o_{i,j}\ x_{i+1,j}] + pP[x_{i,j}\ o_{i+1,j}]$$
$$- \frac{1}{4}P\begin{bmatrix} & x_{i,j+1} & \\ x_{i-1,j} & o_{i,j} & o_{i+1,j} \end{bmatrix} - \cdots$$
$$+ h\Bigg(P[o_{i-1,j}\ -\ o_{i+1,j}]$$

$$+ P\begin{bmatrix} o_{i,j+1} & \\ - & o_{i+1,j} \end{bmatrix} + \cdots$$
$$- 6P[o_{i,j}\ o_{i+1,j}]\Bigg). \tag{3b}$$

For further insight into the exact reduction procedure for the autocatalytic particle creation terms, see Ref. [29], which treats the QCP with $h = 0$. For the QCP with $h > 0$, additional terms corresponding to hopping appear in both the $P[o_{i,j}]$ and $P[o_{i,j}\ o_{i+1,j}]$ equations. These have been simplified by exact reduction [31,32]. Note that for vertical interfaces or more general states which are translationally invariant in the vertical direction, probabilities are independent of j leading to significant simplification of Eqs. (3); a different simplification applies for diagonal interfaces (cf. Ref. [29]).

C. Mean-field behavior

As noted above, in the regime of very large hop rate h, where the system is well stirred, all multisite configuration probabilities factorize in terms of constituent single-site probabilities. The site-dependent particle concentration, $C_{i,j} = P[x_{i,j}] = 1 - P[o_{i,j}]$, will vary slowly with position reflecting a characteristic length for spatial inhomogeneities on the order of $h^{1/2}$. Thus, it is natural to introduce a coarse-grained continuum concentration $C(\underline{r} = (i,j)a)$ for lattice constant "a," leaving implicit the t dependence. Then, applying the factorization to Eq. (3a), it immediately follows that the evolution of this concentration is described exactly as $h \to \infty$ by the mean-field RDE [18,27]

$$\partial C/\partial t = R(C) + D\nabla^2 C. \tag{4}$$

In Eq. (4), $R(C) = -pC + C^2(1-C)$ describes the cubic mean-field kinetics, and $D = a^2 h$ denotes the diffusion coefficient. One finds a stable active steady state satisfying $p = C(1-C)$, so that $C_{eq} = \frac{1}{2} + \frac{1}{2}(1-4p)^{1/2}$ for $0 \le p \le p_{s+} = \frac{1}{4}$, as well as a stable vacuum steady state $C = 0$ for all p. Here, $p_{s+} = \frac{1}{4}$ denotes the (mean-field) upper spinodal. Note that one can write

$$R(C) = -d/dC\,U(C), \quad \text{with } U(C) = \frac{1}{2}pC^2 - \frac{1}{3}C^3 + \frac{1}{4}C^4. \tag{5}$$

The effective free-energy density, $U(C)$, has a double-well form for $0 \le p < p_{s+} = \frac{1}{4}$, and reduces to $U(C) = \frac{1}{4}C^2(2/3 - C)^2$ at equistability $p = p_e = 2/9$ with equal well heights [18,27]. To elucidate the significance of p_e, we note that the velocity $V(p)$ with which the active state displaces the vacuum state in the bistable region can be determined by analysis of the RDE (4). One finds that this velocity satisfies $V(p) \propto D^{1/2}[3(1-4p)^{1/2} - 1]$ for $0 \le p \le p_{s+} = \frac{1}{4}$ and vanishes at $p = p_e = 2/9$ [3,18]. Thus, p_e corresponds to the location of the discontinuous transition for the QCP with hopping in the limit as $h \to \infty$, i.e., the above analysis constitutes the nonequilibrium analog of a Maxwell construction. See Fig. 2(b) for a plot of mean-field steady-state behavior.

TABLE I. KMC simulation and pair-approximation results for p_e, p_{s+}, the width of the metastable regime $\Delta p_{s+} = p_{s+} - p_e$, and KMC results for c_{nuc} in the QCP with particle hop rate $h \geq 0$. Note that KMC values for Δp_{s+} and c_{nuc} vary nonmonotonically for small h with $\Delta p_{s+} = 0.005$ and $c_{nuc} = 0.012$ for $h = 0.1$, and $\Delta p_{s+} = 0.006$ and $c_{nuc} = 0.048$ for $h = 0.4$. See Ref. [18] for further discussion.

	p_e	p_{s+}	Δp_{s+}	c_{nuc}
$h=0$ KMC	0.094	0.101	0.007	0.024
$h=0$ pair approx.	0.1083	0.1250	0.0167	
$h=1$ KMC	0.199	0.213	0.014	0.14
$h=1$ pair approx.	0.2079	0.2329	0.0250	
$h=4$ KMC	0.215	0.236	0.021	0.36
$h=4$ pair approx.	0.2181	0.2451	0.0270	
$h=\infty$ exact	0.2222${}^{\bullet}$	0.2500	0.0278	∞

III. SIMULATION RESULTS: SPINODAL POINTS, POISONING KINETICS, AND INTERFACE PROPAGATION

We first describe results from conventional KMC simulations which were performed primarily to characterize the poisoning kinetics for $p > p_e$, i.e., the approach of the system to the vacuum state, for our QCP realization of Schloegl's model. In these simulations, processes are implemented with probabilities in proportion to the physical rates. Simulations become less efficient for increasing h, as more time is spent on implementing hopping of an often high concentration of mobile particles. This KMC simulation challenge for large hop rates applies for both idealized and realistic atomistic models of reaction-limited processes.

A. Nucleation-mediated poisoning

Of particular interest in this study is the poisoning kinetics of the QCP for moderate hop rates h for $p > p_e$ and specifically around the effective spinodal point. As $p > p_e$ increases, one should find a transition from slow poisoning mediated by nucleation and growth of supercritical vacuum droplets within a metastable active state to a faster poisoning associated with spinodal decomposition [17,18]. Thus, our first strategy to estimate the spinodal location comes from direct inspection of simulation images of evolving (poisoning) configurations for various p's.

Previous simulation studies have determined the variation with h of the annihilation rate, $p_e = p_e(h)$, below which a stable active steady state exists [18], specifically $p_e(h) = 0.0944$, 0.1990, 0.2150, and 0.2222${}^{\bullet}$ for $h = 0$, 1, 4, and ∞, respectively (see Table I). In addition, these studies have determined a distinct annihilation rate, $p_f = p_f(h)$, such that $p_f(h) < p_e(h)$ and both active and vacuum states are stable against local perturbations by the other state in the regime $p_f(h) < p < p_e(h)$ [16–18]. The model is described as exhibiting generic two-phase coexistence in this regime. The origin of this behavior resides in the feature that the equistability point for planar interfaces separating active and vacuum states depends on the orientation of the interface. Specifically, $p_e(h)$ is the equistability point for diagonal interfaces and $p_f(h)$ for horizontal or vertical interfaces. From the KMC
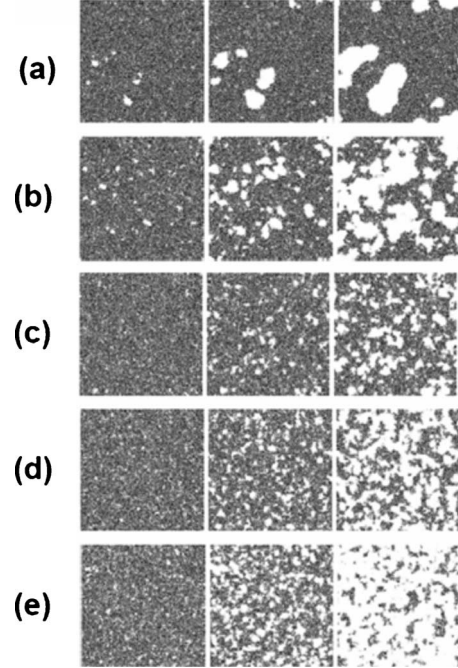

FIG. 3. Simulated evolution in the QCP with $h=1$ starting from a filled 1024×1024 site lattice (which quickly evolves to a metastable active state) for (a) $p=0.208$; $t=480$, 960, 1440; (b) $p=0.210$; $t=240$, 480, 720; (c) $p=0.212$; $t=96$, 192, 288; (d) $p=0.213$; $t=96$, 192, 288; and (e) $p=0.214$; $t=96$, 192, 288.

simulation, one finds that $p_e(h=0+) = 0.094\,43$ and $p_f(h=0+) = 0.0869$ [16]. Thus, the width of the generic two-phase coexistence region satisfies $p_e - p_f = 0.0075$ for $h=0+$, but it quickly decreases to very small values $p_e - p_f < 0.0001$ for $h \geq 0.02$ [18].

In Fig. 3, we show evolution in the QCP with $h=1$ from a completely filled lattice for various $p > p_e(h=1) \approx 0.197$. In Figs. 3(a) and 3(b) for $p \leq 0.210$, it is clear that poisoning occurs via nucleation and growth of vacuum droplets. However, as p increases to 0.214, Figs. 3(c)–3(e) suggest a transition in the mechanism of poisoning. Tentatively, we assign an effective spinodal point of $p_{s+}(h=1) \approx 0.213$. In Fig. 4, we show the analogous evolution for the QCP with $h=4$ for various $p > p_e(h=4) \approx 0.215$. Figures 4(a) and 4(b) for $p \leq 0.234$ reveal nucleation-mediated poisoning, but Figs. 4(c)–4(e) suggest a transition to a different mechanism for higher p. Tentatively, we assign an effective spinodal point of $p_{s+}(h=4) \approx 0.236$ (see Table I).

A more detailed characterization of nucleation-mediated poisoning for $p_e < p < p_{s+}$ is possible. One can utilize concepts from Avrami theory [33] combined with recent postulates for the nucleation rate in these nonequilibrium systems [17,18,21]. We propose that the nucleation rate for supercritical droplets of the vacuum state within the metastable active state has the form $k_{nuc} \propto \exp(-c_{nuc}/\delta p_e)$, where $\delta p_e = p - p_e$. After nucleation, these droplets grow with a velocity scaling like $V_{grow} \propto \delta p_e$. Then, according to Avrami theory, nucleation kinetics is controlled by a characteristic time $\tau_{nuc} \propto (V_{grow})^{-2/3}(k_{nuc})^{-1/3}$. Specifically, after a "brief" transient period where the concentration quickly reaches a metastable state value C_m, one has [33]
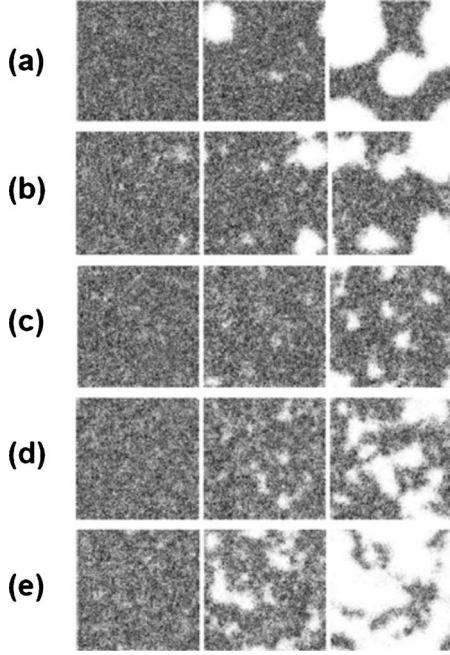
FIG. 4. Simulated evolution in the QCP with $h=4$ starting from a filled 512×512 site lattice (which quickly evolves to a metastable active state) for (a) $p=0.232$; $t=290, 580, 870$; (b) $p=0.234$; $t=116, 232, 348$; (c) $p=0.235$; $t=58, 116, 174$; (d) $p=0.236$; $t=58, 116, 174$; and (e) $p=0.237$; $t=58, 116, 174$.

$$C(t)/C_m \approx \exp[-A(t/\tau_{nuc})^3], \quad \text{choosing}$$

$$\tau_{nuc} = (\delta p_e)^{-2/3} \exp[c_{nuc}/(3 \delta p_e)]. \tag{6}$$

Figure 5 confirms this behavior for nucleation-mediated poisoning kinetics for the QCP with $h=1$ for $p=0.208-0.211$ above $p_e(h=1)=0.199$ and below $p_{s+}(h=1) \approx 0.213$. We extract an estimate of $c_{nuc}(h=1) \approx 0.14$ which reflects the magnitude of the effective barrier for nucleation of supercritical vacuum droplets [18]. We have performed a similar analysis of nucleation-mediated poisoning kinetics with $h=4$ for p
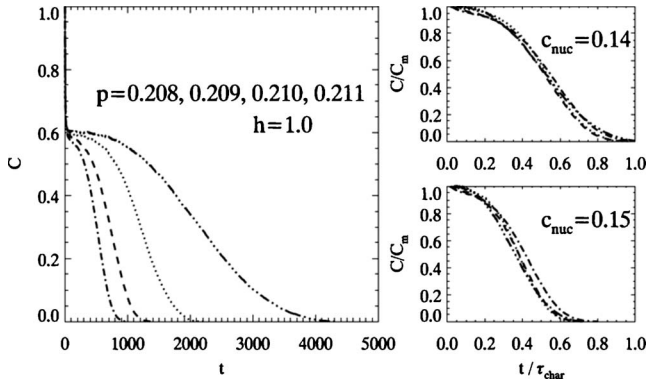

FIG. 5. Simulation results for nucleation-mediated poisoning kinetics in the QCP for $h=1$ for $p=0.208-0.211$ between $p_e(h=1)=0.197$ and $p_{s+}(h=1) \approx 0.213$. Curves in the right frames are collapsed by rescaling in terms of a characteristic time τ_{char}. We choose $\tau_{char}=\tau_{nuc}$ from Eq. (6) and adjust the parameter c_{nuc} to achieve optimal collapse (given here by $c_{nuc}=0.14$ rather than 0.15).

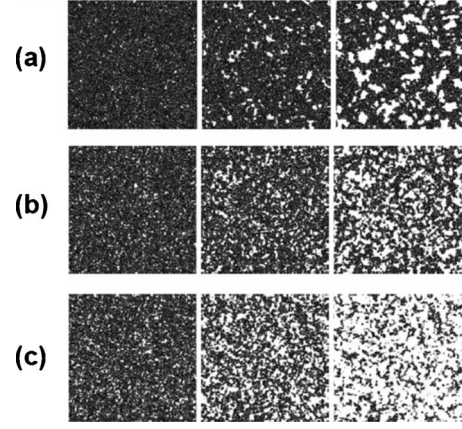FIG. 6. Simulated evolution in the QCP with $h=0$ starting from a filled 1024×1024 site lattice (which quickly evolves to a metastable active state) for (a) $p=0.098$; $t=455, 2275, 4090$; (b) $p=0.100$; $t=455, 910, 1365$; and (c) $p=0.101$; $t=455, 910, 1365$.

$=0.233-0.235$ above $p_e(h=4)=0.215$ and below $p_{s+}(h=4) \approx 0.236$. As expected [18], we extract an even higher estimate of $c_{nuc}(h=4) \approx 0.36-0.37$. Note that significantly smaller values of c_{nuc} were obtained previously for h between 0 and 0.4 (see Table I) [18].

As an aside, we remark that for $h=0$, previous studies have indicated very weak metastability. Indeed, inspection of evolving configurations during poisoning for $h=0$ does not reveal such a clear distinction between nucleation-mediated poisoning and spinodal decomposition (see Fig. 6). Analysis of rapid poisoning kinetics for $p>p_{s+}$ suggests that perhaps $p_{s+}(h=0)=0.100-0.101$.

B. Rapid poisoning via spinodal decomposition

A second strategy to assess the location of effective spinodal point is based on the idea that the rate of rapid poisoning in the regime $p>p_{s+}$ should depend primarily on the distance, $\delta p_{s+}=p-p_{s+}>0$, above an effective spinodal. Specifically, $C(t)$ should roughly have the form $C(t) \approx c(\delta p_{s+}t)$, so that curves for C versus $\delta p_{s+}t$ for different p's should collapse for the appropriate choice of p_{s+} [14,17,18]. The application of this idea requires selection of a suitable regime $(p_{s+}<)p_{min}<p<p_{max}$ in which to analyze the kinetics. In fact, we choose two different regimes for higher or lower $\Delta = p_{min} - p_{s+}$ based on the above initial estimates of p_{s+}. We do this in order to assess the dependence of our refined estimates based on poisoning kinetics of p_{s+} on Δ. Figure 7(a) shows poisoning kinetics in the QCP for $h=1$ for a range of $p=0.220-0.235$ ($\Delta \approx 0.007$) above $p_e(h=1)=0.199$, suggesting $p_{s+}(h=1)=0.207-0.208$. However, kinetics shown in Fig. 7(b) for $p=0.215-0.225$ ($\Delta \approx 0.002$) suggests that $p_{s+}(h=1)=0.209-0.210$. A similar analysis of poisoning kinetics in the QCP for $h=4$ for a range of $p=0.245-0.270$ ($\Delta \approx 0.009$) above $p_e(h=4)=0.215$ suggests that $p_{s+}(h=4)=0.226-0.227$. However, kinetics for $p=0.240-0.260$ ($\Delta \approx 0.004$) suggests that $p_{s+}(h=4)=0.228-0.229$. Thus, the estimate of p_{s+} appears to consistently increase as Δ becomes smaller. In Sec. IV, with the aid of the analytical pair approximation for model kinetics, we will discuss how to ob-
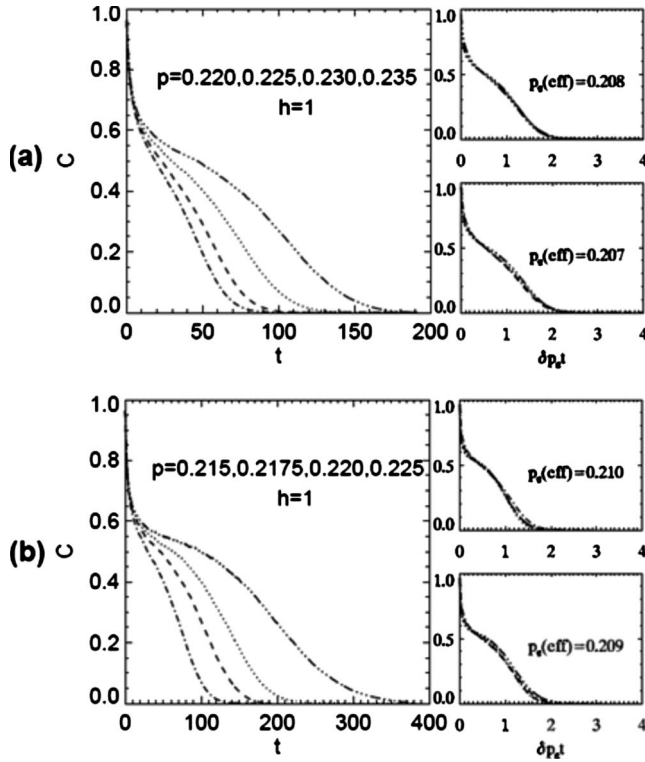
FIG. 7. Simulation results for "rapid" poisoning kinetics in the QCP for $h=1$ for p above $p_{s+}(h)$: (a) $p=0.220-0.235$ data suggesting that $p_{s+}(h=1)=0.207-0.208$; (b) $p=0.215-0.225$ data suggesting that $p_{s+}(h=1)=0.209-0.210$.

tain a refined estimate of p_{s+} accounting for this dependence on Δ.

C. Interface propagation

Finally, we comment on yet another third strategy to provide insight into the effective p_{s+}. This strategy is motivated by the mean-field results described at the end of Sec. II which suggest that the velocity of propagation, $V(p)<0$, of the vacuum state displacing the metastable active state for $p>p_e$ might have distinctive (e.g., singular) behavior approaching p_{s+}. One complication in the lattice-gas realization of the model is that such propagation is transient in the sense that the metastable active state eventually spontaneously poisons. This becomes more of an issue for p approaching p_{s+} (the regime of primary interest here) where spontaneous nucleation and growth of the vacuum state becomes more facile. To partly ameliorate this problem, we have previously adopted a percolation-theoretic approach defining the interface as the set of empty sites connected to the bulk vacuum state which have filled neighbors [18]. This allowed us to ignore possibly large droplets of the vacuum state nucleated ahead of the front in the metastable active state. However, eventually the vacuum droplets embedded in the metastable active state grow and percolate, causing an artificial divergence of the velocity of interface defined by the above algorithm.

To avoid this complication, here we adopt a different and less conventional, but simpler definition of the interface, as
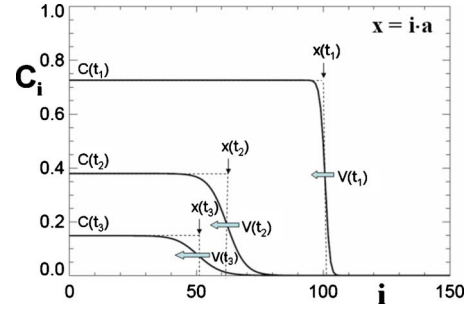

FIG. 8. (Color online) Schematic for determination of the location $x(t)$ of a vertical interface between the vacuum state and an initially filled "poisoning state" from the concentration profiles in the QCP for $p>p_e$. Profiles are shown as solid curves passing through discrete average concentrations $C_i=\langle C_{i,j}\rangle_j$ for column i, where (i,j) is the site label on the square lattice. $x(t)$ matches the location of the reference sharp interface (dashed curves), so that $\Sigma_i C_i(t)=\Sigma_{i<x(t)}C(t)$, where $C(t)\to 0$ as $t\to\infty$ denotes the concentration of a uniform initially filled state. Profiles shown are taken from pair-approximation simulations with $h=1$ and $p=0.235$ exceeding $p_{s+}\approx 0.233$. An analogous definition is possible for other interface orientations.

well as of its location and thus velocity. We initialize a (large finite) system with a sharp planar interface separating the vacuum state on one side and a completely filled lattice on the other. Then, we determine the subsequent mean location of this interface by comparing the concentration profile (averaged along the interface) with that of a reference sharp interface having the vacuum state on one side and an appropriate evolving "benchmark" uniform state on the other. This benchmark uniform state corresponds to a poisoning state which started from an initially completely filled state (see the schematic in Fig. 8). This strategy gives a well-defined interface location even for $p>p_{s+}$ where the nonvacuum state poisons very rapidly. To interpret simulation results, two observations should be made regarding this definition of interface location and velocity motivated by behavior in a mean-field model: (i) as $p\to p_{s+}$ from below, one expects that it will take longer for the interface to reach its true asymptotic velocity (which is nonanalytic at p_{s+}) and (ii) for $p>p_{s+}$, the propagating front is expected to accelerate (with changing shape).

Simulation results for this interface velocity $V(p)$ versus p in the QCP with $h=1$ are shown in Fig. 9 where $V(p)$ is determined as the difference between interface location at initial time $t_i\approx 60$ and that at a range of final times t_f. Note that $V(p)$ for $h=1$ is effectively independent of interface orientation, and the p value where $V(p)=0$ corresponds to $p_e(h=1)\approx p_f(h=1)$ (see the inset to Fig. 9). The results for $V(p)$ are largely independent of t_f up to $p\approx 0.212$, but then $|V(p)|$ becomes larger for longer t_f and for higher p. This is consistent with mean-field-type acceleration of the front for $p>p_{s+}$. These observations suggest that $p_{s+}(h=1)\approx 0.212$, reasonably consistent with the estimate from Fig. 3.

To summarize, we have introduced three distinct strategies to assess the location of the effective spinodal point. These produce quite consistent estimates, e.g., $p_{s+}(h=1)\approx 0.213$, $0.209-0.210$ (refined to 0.213 below in Sec. IV),
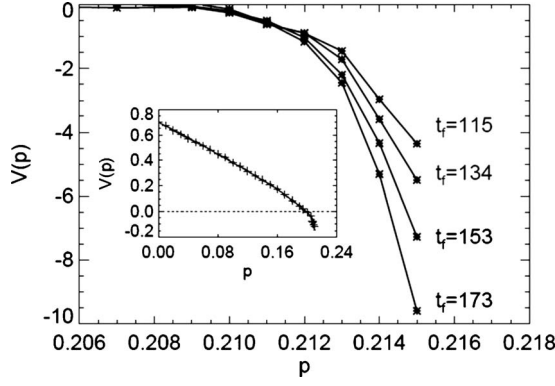
FIG. 9. Simulation results for the propagation velocity $V(p)$ for an interface between vacuum and poisoning states in the QCP with $h=1$ defined as in Fig. 6 where velocity is measured as the difference in location between times $t_i=60$ and t_f (shown). Results depend on t_f just below and above $p=p_{s+}\approx 0.213$. Inset: $V(p)$ over a broader range of p.

and 0.212 from the first, second, and third strategies, respectively, recalling that $p_e(h=1)\approx 0.197$.

IV. PAIR-APPROXIMATION RESULTS: SPINODAL POINTS, POISONING KINETICS, AND INTERFACE PROPAGATION

The lowest-order site approximation to the exact hierarchical master equations ignores all spatial correlations and adopts a mean-field factorization of multisite probabilities in terms of constituent single-site probabilities. Unfortunately, this approximation for spatially homogeneous states completely fails to capture any h dependence of the reaction kinetics, a feature which is of primary interest here. However, this h dependence is described at least approximately by higher-order approximations. Here, we consider only the pair approximation [29,34].

A. Spatially uniform states

Starting with the hierarchical master equations (2) for spatially uniform states, this Kirkwood-type approximation factorizes multisite probabilities in the particle creation terms as products of the m constituent pair probabilities and divides by $P[o]^{m-1}$ to avoid overcounting of the shared central empty site. In addition, hopping terms involving the probabilities of separated pairs of empty sites are factorized as $P[o]^2$. Since $P[x]=1-P[o]$ and $P[x\ o]=P[o]-P[o\ o]$, the pair approximation can be written to yield the closed pair of equations

$$d/dtP[o]=pP[x]-P[x\ o]^2/P[o]$$
$$=p(1-P[o])-(P[o]-P[o\ o])^2/P[o], \quad (7a)$$

$$d/dtP[o\ o]=2pP[x\ o]-P[x\ o]^2P[o\ o]/P[o]^2$$
$$+6h(P[o]^2-P[o\ o])$$
$$=2p(P[o]-P[o\ o])-(P[o]$$
$$-P[o\ o])^2P[o\ o]/P[o]^2$$

$$+6h(P[o]^2-P[o\ o]). \quad (7b)$$

Below it is convenient to let $K=P[x\ o]/P[o]$ denote the conditional probability or conditional concentration of finding a particle adjacent to a prescribed empty site. Due to the presence of spatial correlations, K is distinct from the concentration $C=P[x]=1-P[o]$. Then, noting that $P[x\ o]=K(1-C)$ and $P[o\ o]=(1-K)(1-C)$, the pair approximation yields

$$d/dtC=-pC+K^2(1-C), \quad (8a)$$

$$d/dtK+(1-K)(1-C)^{-1}d/dtC$$
$$=[-2p+K(1-K)]K-6h(K-C). \quad (8b)$$

The hopping term in Eq. (8b) forces $K\to C$, as $h\to\infty$, thus eliminating spatial correlations and correctly recovering mean-field behavior. This, of course, is a general feature for reaction-diffusion systems with no particle interactions, as noted in Sec. II C.

Solving Eqs. (8) for the steady-state behavior determines C_{eq} and K_{eq} versus p in the pair approximation including their h dependence. See Fig. 10 for C_{eq} versus p when $h=1$. One strategy is to eliminate C generating a relationship between the "natural" variable K and the parameter p,

$$6h[p-K(1-K)]+(p+K^2)[2p-K(1-K)]=0 \quad \text{or} \quad K=0. \quad (9)$$

This relationship, which in general yields p versus K by solving a quadratic, immediately reveals simple behavior for both $h=0$ and $h\to\infty$. Given the dependence of K on p, one can then assess that for C on p. For example, when $p\ll 1$, one finds that
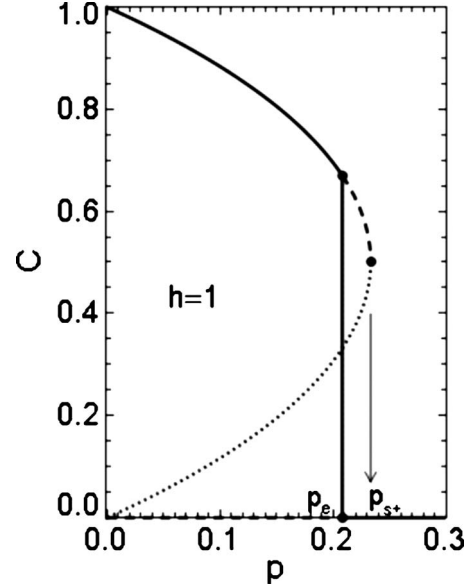

FIG. 10. Steady-state behavior in the pair approximation for the particle concentration $C_{eq}(p)$ versus p with $h=1$. The format and notation are the same as those for Fig. 2.
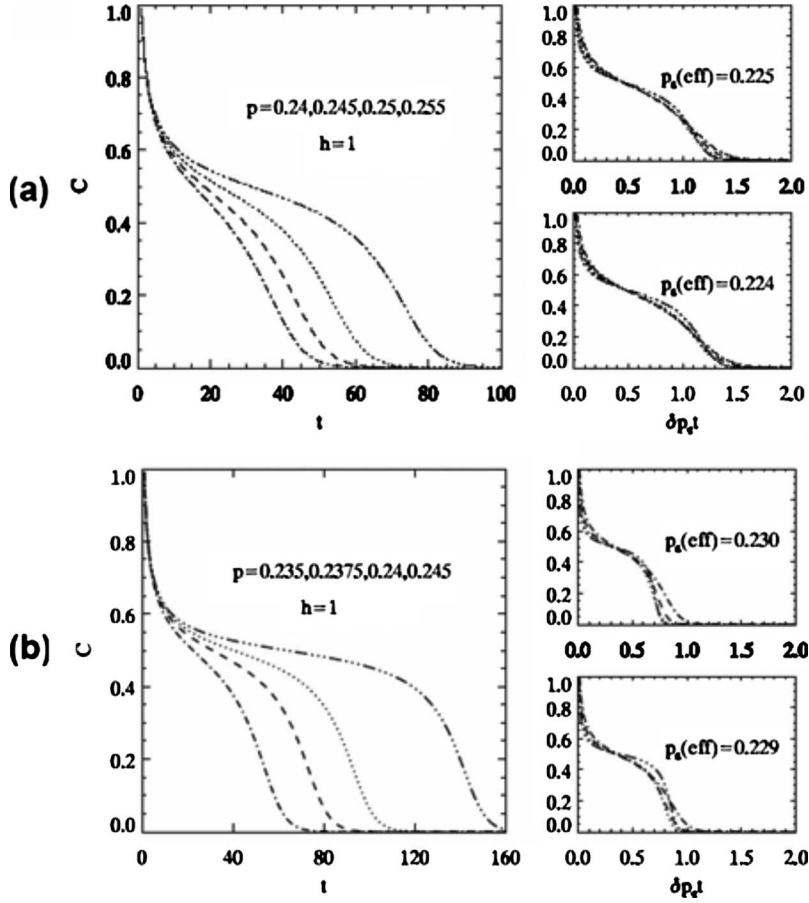
FIG. 11. Pair-approximation results for the poisoning kinetics in the QCP for $h=1$ for (a) $p=0.240-0.255$ data suggesting that $p_{s+}(h=1)=0.224-0.225$; (b) $p=0.235-0.245$ data suggesting that $p_{s+}(h=1)=0.229-0.230$.

$$C_{eq} = 1 - p + O(p^2), \quad K_{eq} = 1 - (2+6h)(1+6h)^{-1}p + O(p^2). \quad (10)$$

The differing linear terms show that spatial correlations persist even for small p when $h<\infty$. Alternatively, one can eliminate p from steady-state form of Eqs. (8) to obtain K_{eq} as a function of C_{eq}, thus obtaining

$$K_{eq} \approx C_{eq}[1 - C_{eq}(1-C_{eq})/(6h)], \quad \text{for } h \gg 1, \quad (11a)$$

$$K_{eq} \approx C_{eq}(2-C_{eq})^{-1}[1 - 6h(2-C_{eq})(1-C_{eq})/C_{eq}]^{-1},$$
$$\text{for } h \ll 1. \quad (11b)$$

Either approach provides insight into spinodal behavior, for example, showing that

$$p_{s+}(\text{pair}) \approx 1/4 - 1/(48h), \quad \text{for } h \gg 1,$$

$$p_{s+}(\text{pair}) \approx 1/8 + h, \quad \text{for } h \ll 1. \quad (12)$$

In addition, one finds a transition in behavior from

$$C_{eq} = \tfrac{1}{2}(1+p)^{-1}[1 + 4p + (1-8p)^{1/2}], \quad \text{for } h=0 \text{ to}$$

$$C_{eq} = \tfrac{1}{2}[1 + (1-4p)^{1/2}], \quad \text{for } h=\infty. \quad (13)$$

Next, we utilize numerical analysis of the pair-approximation equations to provide additional insight into poisoning kinetics for the cases $h=1$ and $h=4$ analyzed by the KMC simulation in Sec. III. Specifically, we analyze the

rapid poisoning kinetics for $p>p_{s+}$ choosing ranges of $p_{min} < p < p_{max}$ for the same distance $\Delta = p_{min} - p_{s+}$ above p_{s+} as in the simulation studies. However, Fig. 11(a) shows pair-approximation kinetics in the QCP for $h=1$ for a range of $p=0.240-0.255$ ($\Delta \approx 0.007$) suggesting that $p_{s+}(h=1) = 0.224-0.225$, and Fig. 11(b) shows $p=0.235-0.245$ ($\Delta \approx 0.002$) suggesting that $p_{s+}(h=1) = 0.229-0.230$. Thus, even the latter small-Δ estimate is about 0.003 below the correct value of $p_{s+}(\text{pair}) \approx 0.2329$ for $h=1$ obtained from an exact steady-state analysis in the pair approximation (see Table I). If this correction is applied to the $\Delta \approx 0.002$ simulations in Fig. 6(b), one obtains a refined simulation estimate of $p_{s+}(h=1) \approx 0.213$ (consistent with direct analysis from Fig. 3). Similar pair-approximation analysis for $h=4$ [35] suggests a refined simulation estimate of $p_{s+}(h=4) \approx 0.235$ (consistent with direct analysis from Fig. 4). Note that these refined estimates deviate from previous cruder estimates [18] for fixed Δ.

B. Spatially nonuniform states

Finally, we discuss the extension of the pair approximation to the description of spatially nonuniform states. In particular, we wish to analyze the propagation of an interface between the active and vacuum states to determine the equistability pressure $p_e(h)$ and related quantities. In addition, we wish to assess the characteristics of interface propagation for $p>p_e(h)$, particularly for $p \approx p_{s+}(h)$ (analogous to the simulation studies in Sec. III). The truncation procedure based on

TABLE II. Pair-approximation results for the QCP with particle hop rate h. Values of p for equistability of vertical interfaces, $p_{eq}(S=\infty)$, and diagonal interfaces, $p_{eq}(S=1)$, between active and vacuum states, and for the upper spinodal, p_{s+}. For $h=4$, we find that $p_{eq}(S) \approx p_e = 0.218\ 094$ and $p_{s+} = 0.245\ 07$.

Pair approx.	$p_{eq}(S=\infty$ or $0)$	$p_{eq}(S=1)=p_e$	p_{s+}
$h=0$	0.1060	0.1083	$1/8=0.1250$
$h=0.01$	0.11759	0.11863	0.13429
$h=0.05$	0.14335	0.14368	0.15997
$h=0.10$	0.16018	0.16035	0.17828
$h=0.20$	0.17776	0.17784	0.19801
$h=0.50$	0.197546	0.197573	0.22078
$h=1.0$	0.207900	0.207909	0.23292

factorization of probabilities naturally extends to the infinite hierarchy (3) for spatially nonuniform states at the level of either the site or pair approximation. In either case, the result is a set of discrete RDEs for the site-dependent particle concentration, and also for related pair probabilities in the case of the pair approximation. An early example of this procedure for a lattice-gas reaction model at the level of the site approximation is found in Ref. [36], and for the QCP with $h=0$ at the level of the site and pair approximations it is found in Ref. [29]. The extension of the latter analysis to include diffusion terms is straightforward and has been implemented here. We present results at the pair-approximation level based on analysis of these coupled discrete RDEs. For special cases of vertical or diagonal interfaces, these can be simplified as in Ref. [29].

We have noted previously that the QCP for $h \geq 0$ exhibits generic two-phase coexistence [16–18]. This feature derives from the property that the equistability or stationarity point, $p=p_{eq}(h,S)$, for a planar interface separating active and vacuum states depends on the orientation or slope S of the interface. This property is preserved in the spatially nonuniform site and pair approximations. Table II shows the dependence of the annihilation rates for stationarity of vertical (or horizontal) interfaces and of diagonal interfaces as a function of h in the pair approximation. Note that p_{eq} for diagonal interfaces corresponds to p_e in the exact QCP. There are some complications associated with propagation failure of vertical interfaces for these discrete RDEs [29,37] which will be discussed elsewhere. However, the main observation here is that pair approximation predicts that the orientation dependence of interface propagation and equistability quickly diminishes with increasing h (although not as quickly as actual model behavior determined from simulations [18]). Thus, this dependence on interface orientation can be ignored for the cases $h=1$ and $h=4$ on which we focus here.

Our primary interest here is in analyzing the variation of velocity of propagation, $V(p)<0$, for $p>p_e$ of an interface between a vacuum state and a state which is initially a filled lattice. Note that $V(p)$ for $h=1$ is effectively independent of interface orientation. This analysis is the analog of the simulation analysis of interface propagation in Fig. 9. Within the pair approximation, this corresponds to the vacuum state displacing the metastable active state for $p_e<p<p_{s+}$ or displac-
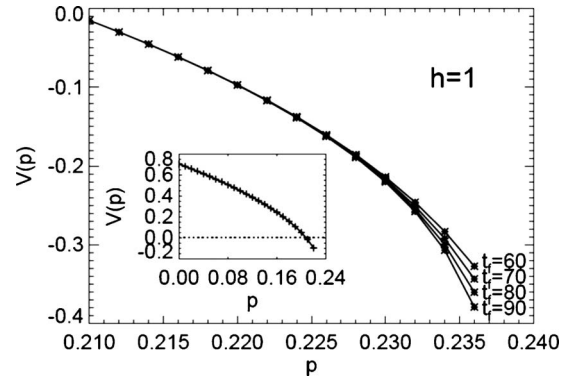

FIG. 12. Pair-approximation results for the propagation velocity $V(p)$ for an interface between vacuum and poisoning states in the QCP with $h=1$ defined as in Fig. 7 where velocity is measured as the difference in location between times $t_i=60$ and t_f (shown). Results depend on t_f just below and above $p=p_{s+}\approx 0.233$. Inset: $V(p)$ over a broader range of p (agreeing well with simulation results in the inset to Fig. 9).

ing a poisoning state for $p>p_{s+}$. Results for $V(p)$ versus p in the QCP with $h=1$, where $p_e(h=1)=0.2079$ and $p_{s+}(h=1)=0.2329$ in the pair approximation, are shown in Fig. 12. Note again that $V(p)=0$ corresponds to $p=p_e(h=1)\approx p_f(h=1)$ (see the inset to Fig. 12). Here, $V(p)$ is determined as the difference between the interface location at initial time $t_i=30$ and that at a range of final times t_f. The result is largely independent of t_f up to $p\approx 0.232$ just below $p_{s+}=0.233$, but $|V(p)|$ becomes larger for longer t_f and for higher p, consistent with acceleration of the front for $p>p_{s+}$. Thus, the behavior is entirely analogous to that in Fig. 9. As an aside, we note the effectiveness of the pair approximation in recovering the simulated behavior of $V(p)$ versus p over a broad range of $0 \leq p \leq p_{s+}$. Compare the insets in Figs. 9 and 12.

V. CONTINUUM RDEs BASED ON THE PAIR APPROXIMATION

Mean-field continuum Langevin reaction-diffusion equations (RDEs) [38,39] have provided a useful conceptual framework for analysis of fluctuation effects in reaction-diffusion systems, where the hop rate is sufficiently large to ensure effective mixing and thus mean-field reaction kinetics, but not so large as to completely quench fluctuations [9]. However, for our analysis of the QCP with moderate particle hop rates, there are significant deviations from mean-field reaction kinetics as reflected in the shift of the spinodal points from the $h \to \infty$ mean-field value of 1/4 toward 1/8. Consequently, we are motivated to incorporate a higher-level pair-approximation description of reaction kinetics into a continuum RDE formulation. One strategy for deriving continuum RDEs without noise terms is to coarse grain the discrete RDEs which follow from the spatially nonuniform form of the exact hierarchical master equations after applying the appropriate factorization approximation. This analysis will not yield noise terms, but these might come from separate consideration of suitable birth-death master equations for discrete populations of relevant "species" in an array of spatial cells [1,38,39].

To coarse grain the discrete RDEs, we start with the form of Eqs. (3) factorized in the pair approximation to yield evolution equations for the site-dependent probabilities of empty sites and adjacent empty pairs at various locations. We then rewrite these in terms of coarse-grained continuum variables to describe their spatial variation after applying suitable Taylor expansions (cf. Ref. [40]). Note that concentration gradients can induce different nearest-neighbor correlations in horizontal and vertical directions, so we use two corresponding variables. Leaving implicit the t dependence, the complete set of variables is

$$U(\underline{r} = (i,j)a) = P[o_{i,j}],$$
$$V\left(\underline{r} = \left(i + \tfrac{1}{2}, j\right)a\right) = P[o_{i,j} \ o_{i+1,j}],$$
$$W\left(\underline{r} = \left(i, j + \tfrac{1}{2}\right)a\right) = P[o_{i,j} \ o_{i,j+1}], \qquad (14)$$

where the location $\underline{r}$ for the pair probabilities is chosen midway between the pair of sites, and again a is the lattice constant. Examples of Taylor expansions used in developing the equation for $U(\underline{r}=(i,j)a)$ are

$$P[o_{i\pm1,j}] = U(\underline{r}) \pm aU_x(\underline{r}) + \tfrac{1}{2}a^2 U_{xx}(\underline{r}) + \cdots, \quad \text{for } \underline{r} = (i,j)a,$$
$$(15a)$$

$$P[o_{i,j} \ o_{i,j\pm1}] = V(\underline{r}) \pm \tfrac{1}{2}aV_y(\underline{r}) + \tfrac{1}{8}a^2 V_{yy}(\underline{r}) + \cdots,$$
$$\text{for } \underline{r} = (i,j)a. \qquad (15b)$$

An example of an expansion used in developing the equation for $V(\underline{r}=(i+\tfrac{1}{2},j)a)$ is

$$P[o_{i+1,j} \ o_{i+1,j\pm1}] = W(\underline{r}) + \tfrac{1}{2}aW_x(\underline{r}) \pm \tfrac{1}{2}aW_y(\underline{r}) + \tfrac{1}{8}a^2 W_{xx}(\underline{r})$$
$$+ \tfrac{1}{8}a^2 W_{yy}(\underline{r}) \pm \tfrac{1}{4}a^2 W_{xy}(\underline{r}) + \cdots,$$
$$\text{for } \underline{r} = \left(i + \tfrac{1}{2}, j\right)a. \qquad (16)$$

Thus, upon substitution of such expressions into the pair-approximation factored form of Eqs. (3), one obtains

$$\partial/\partial t U = p(1-U) - U^{-1}(U-V)(U-W) + 1/8a^2(U-V)W_{yy}$$
$$+ 1/8a^2(U-W)V_{xx} + a^2 h(U_{xx} + U_{yy}), \qquad (17a)$$

$$\partial/\partial t V = 2p(U-V) - U^{-2}V(U-V)(U-W) + 6h(U^2 - V)$$
$$+ a^2 hU\left(7/2 U_{xx} + \tfrac{1}{2}U_{yy}\right) + \tfrac{1}{4}a^2 p U_{xx} + \text{other}, \quad (17b)$$

where "other" denotes additional $O(a^2)$ terms. The W equation follows from that for V by rotational symmetry. Note that for a spatially uniform system where $V=W$, Eqs. (17) recover the pair-approximation kinetics (7) and steady states described previously.

Addition of noise terms to RDEs of the above type would allow simulation at the level of the pair approximation of metastability and nucleation-mediated poisoning (phenomena described in Sec. III and quantified in Fig. 5). Standard procedures are available at the mean-field level to generate such noise terms which include separate nonconserved contributions due to particle annihilation and creation, and conserved contributions due to diffusion [18,38,39]. For a formulation at the level of the pair approximation, insight into the noise terms associated with particle annihilation and cre-

ation might come from analysis of appropriate master equations describing the evolution of finite populations of, say, *oo* and *xo* pairs of sites within a finite system. Then, coarse graining to obtain the associated Fokker-Planck equations would indicate the form of multiplicative Langevin noise terms to be included in the RDEs for the corresponding coarse-grained pair probabilities. Details will be presented elsewhere [41].

VI. CONCLUSIONS

We have analyzed a stochastic realization of Schloegl's second model for autocatalysis with particle diffusion on a square lattice, also known as the quadratic contact process. This model provides an ideal testing ground to explore fundamental issues related to discontinuous phase transitions and associated metastability phenomena in nonequilibrium reaction-diffusion models. Based on analysis for equilibrium Ising-type models, one does not expect that an unambiguous or precise definition is possible for the spinodal point in our nonequilibrium model for an infinite lattice. Nonetheless, the concept of a spinodal appears to provide a useful tool for analyzing poisoning kinetics, particularly for moderate or large hop rates.

Our combination of simulation and pair-approximation analysis is effective in characterizing behavior associated with metastability. In particular, we are able to determine the location of the effective spinodal point as a function of particle hop rate. This analysis in part exploited the strategy of analyzing the poisoning kinetics, akin to dynamical analyses of spinodal behavior in equilibrium systems [4,5]. In addition, we explore interface propagation in the vicinity of an effective spinodal point to assess its location. In the context of lattice-gas reaction models, there have been many studies of interface propagation between a stable active state and a poisoned adsorbing state [9,14–18]. This is analogous to the propagation of trigger waves between two stable states in mean-field models [8]. There have also been many lattice-gas model studies of interface propagation between stable and unstable states which exhibits more pathological features [42]. The analysis here is closer to the former case, although propagation of the poisoned state into the metastable active state is a transient phenomenon.

Finally, this work also promotes the possibility of developing coarse-grained stochastic reaction-diffusion equations at a level beyond the standard mean-field treatment. Such equations could describe behavior associated with metastability for moderate hop rates where mean-field kinetics is not accurate.

[1] J. D. Gunton and M. Droz, *Introduction to the Theory of Metastable and Unstable States*, Springer Lecture Notes in Physics (Springer, Berlin, 1983), Vol. 183.

[2] J. D. Gunton, M. San Miguel, and P. S. Sahni, in *Phase Transitions and Critical Phenomena*, edited by J. L. Lebowitz and C. Domb (Academic Press, London, 1983).

[3] H. E. Stanley, *Introduction to Phase Transitions and Critical Phenomena* (Oxford University Press, Oxford, 1971).

[4] R. H. Schonmann and S. B. Shlosman, Commun. Math. Phys. **194**, 389 (1998).

[5] S. Shlosman, Physica A **263**, 180 (1999).

[6] S. Friedli and C.-E. Pfister, Phys. Rev. Lett. **92**, 015702 (2004).

[7] G. Nicolis and I. Prigogine, *Self-Organization in Non-Equilibrium Systems* (Wiley, New York, 1977).

[8] A. S. Mikhailov, *Foundations of Synergetics I* (Springer, Berlin, 1990).

[9] J. W. Evans, D.-J. Liu, and M. Tammaro, Chaos **12**, 131 (2002).

[10] J. Marro and R. Dickman, *Nonequilibrium Phase Transitions in Lattice Models* (Cambridge University Press, Cambridge, England, 1999).

[11] H. Hinrichsen, Adv. Phys. **49**, 815 (2000).

[12] G. Odor, Rev. Mod. Phys. **76**, 663 (2004).

[13] R. M. Ziff, E. Gulari, and Y. Barshad, Phys. Rev. Lett. **56**, 2553 (1986).

[14] J. W. Evans and T. R. Ray, Phys. Rev. E **50**, 4302 (1994).

[15] R. H. Goodman, D. S. Graff, L. M. Sander, P. Leroux-Hugon, and E. Clément, Phys. Rev. E **52**, 5904 (1995).

[16] D.-J. Liu, X. Guo, and J. W. Evans, Phys. Rev. Lett. **98**, 050601 (2007).

[17] X. Guo, D.-J. Liu, and J. W. Evans, Phys. Rev. E **75**, 061129 (2007).

[18] X. Guo, D.-J. Liu, and J. W. Evans, J. Chem. Phys. **130**, 074106 (2009).

[19] J. W. Evans and M. S. Miesch, Phys. Rev. Lett. **66**, 833 (1991).

[20] E. Loscar and E. V. Albano, Rep. Prog. Phys. **66**, 1343 (2003).

[21] E. Machado, G. M. Buendia, and P. A. Rikvold, Phys. Rev. E **71**, 031603 (2005).

[22] M. Tammaro, M. Sabella, and J. W. Evans, J. Chem. Phys. **103**, 10277 (1995).

[23] F. Schloegl, Z. Phys. **253**, 147 (1972).

[24] P. Grassberger, Z. Phys. B: Condens. Matter **47**, 365 (1982).

[25] J. P. Boon, D. Dab, R. Kapral, and A. Lawniczak, Phys. Rep. **273**, 55 (1996).

[26] S. Prakash and G. Nicolis, J. Stat. Phys. **86**, 1289 (1997).

[27] R. Durrett, SIAM Rev. **41**, 677 (1999).

[28] P. A. Rikvold, H. Tomita, S. Miyashita, and S. W. Sides, Phys. Rev. E **49**, 5080 (1994).

[29] X. Guo, J. W. Evans, and D.-J. Liu, Physica A **387**, 177 (2008). Note the error in labeling of sites in the last two loss terms in Eq. (17) of this reference. One should replace i with $i-1$.

[30] J. W. Evans, Rev. Mod. Phys. **65**, 1281 (1993).

[31] J. W. Evans and D. K. Hoffman, Phys. Rev. B **30**, 2704 (1984).

[32] R. Kutner, Phys. Lett. **81A**, 239 (1981).

[33] M. Avrami, J. Chem. Phys. **7**, 1103 (1939); **8**, 212 (1940); **9**, 177 (1941).

[34] R. Dickman, Phys. Rev. A **34**, 4246 (1986).

[35] Pair-approximation analysis of kinetics for $h=4$ for a range of $p=0.254-0.279$ ($\Delta \approx 0.009$) suggests that $p_{s+}(h=4)=0.234-0.235$, but for $p=0.249-0.269$ ($\Delta \approx 0.004$) it suggests that $p_{s+}(h=4)=0.239-0.240$. The latter is 0.005 below the exact value of p_{s+}(pair) ≈ 0.2451 for $h=4$.

[36] P. Fischer and U. M. Titulaer, Surf. Sci. **221**, 409 (1989).

[37] D.-J. Liu, C.-J. Wang, X. Guo, and J. W. Evans (unpublished).

[38] M. Hildebrand and A. S. Mikhailov, J. Phys. Chem. **100**, 19089 (1996).

[39] M. Hildebrand, A. S. Mikhailov, and G. Ertl, Phys. Rev. Lett. **81**, 2602 (1998).

[40] Y. De Decker, G. A. Tsekouras, A. Provata, Th. Erneux, and G. Nicolis, Phys. Rev. E **69**, 036203 (2004).

[41] Y. De Decker, X. Guo, and J. W. Evans (unpublished).

[42] C. R. Doering, C. Mueller, and P. Smereka, Physica A **325**, 243 (2003).